VFT to Arrhenius crossover at the dynamic glass transition of an epoxy network as revealed by dielectric experiments in continuous immersion

Aurélien Roggero, Nicolas Caussé, Nadine Pébère, Eric Dantras

▶ **To cite this version:**

Aurélien Roggero, Nicolas Caussé, Nadine Pébère, Eric Dantras. VFT to Arrhenius crossover at the dynamic glass transition of an epoxy network as revealed by dielectric experiments in continuous immersion. Polymer, 2022, 241, pp.124542. 10.1016/j.polymer.2022.124542 . hal-03599685

HAL Id: hal-03599685
https://hal.science/hal-03599685

Submitted on 7 Mar 2022

HAL is a multi-disciplinary open access archive for the deposit and dissemination of scientific research documents, whether they are published or not. The documents may come from teaching and research institutions in France or abroad, or from public or private research centers.

L'archive ouverte pluridisciplinaire **HAL**, est destinée au dépôt et à la diffusion de documents scientifiques de niveau recherche, publiés ou non, émanant des établissements d'enseignement et de recherche français ou étrangers, des laboratoires publics ou privés.

OATAO
Open Archive Toulouse Archive Ouverte

Open Archive Toulouse Archive Ouverte (OATAO)

OATAO is an open access repository that collects the work of Toulouse researchers and makes it freely available over the web where possible

This is an author's version published in: http://oatao.univ-toulouse.fr/28782

Official URL: https://doi.org/10.1016/j.polymer.2022.124542

To cite this version:

Roggero, Aurélien and Caussé, Nicolas and Pébère, Nadine and Dantras, Eric *VFT to Arrhenius crossover at the dynamic glass transition of an epoxy network as revealed by dielectric experiments in continuous immersion.* (2022) Polymer, 241. 124542. ISSN 0032-3861

Any correspondence concerning this service should be sent to the repository administrator: tech-oatao@listes-diff.inp-toulouse.fr

VFT to Arrhenius crossover at the dynamic glass transition of an epoxy network as revealed by dielectric experiments in continuous immersion

Aurélien Roggero [a,b,*], Nicolas Caussé [b], Nadine Pébère [b], Eric Dantras [c]

[a] Université de Lyon, CNRS, UMR 5223, Ingénierie des Matériaux Polymères, UCBL, INSA, UJM, F-69621, Villeurbanne Cedex, France
[b] Université de Toulouse, CIRIMAT, UPS/INPT/CNRS, ENSIACET, 4 allée Emile Monso, BP44362, 31030, Toulouse Cedex 4, France
[c] Université de Toulouse, CIRIMAT, Physique des Polymères, Université Paul Sabatier, Bât. 3R1 B2, 118 route de Narbonne, 31062, Toulouse cedex 9, France

ARTICLE INFO

Keywords:
Molecular mobility
Glass transition
Plasticization
Water interaction
Impedance spectroscopy

ABSTRACT

The influence of water sorption on the α-relaxation of an epoxy network was studied by performing impedance measurements in continuous immersion (in aqueous solution) at various temperatures in the range [20; 80] °C. Relaxation times associated with the α-relaxation were found to shift towards lower temperatures as a result of plasticization, accompanied by a decrease in the relaxation strength. The most striking feature of the impedance measurements was a crossover from a Vogel-Fulcher-Tammann (VFT) to an Arrhenius dependence of the relaxation times upon cooling, in the vicinity of the glass transition of the epoxy network. Complementary experimental techniques (namely differential scanning calorimetry, dielectric spectroscopy, thermally stimulated currents) were used on dry and wet epoxy samples to better understand the physical origin of this crossover. Various scenarios were discussed; the most convincing involved confinement-like effects. The deviation from VFT behaviour below T_g was possibly due to long-living H-bonds between the epoxy network and water molecules, which limited the cooperativity of the α-relaxation. The water molecules H-bonding to the network localized the mobility of the main chain, as confirmed by thermally stimulated currents performed on a wet sample.

1. Introduction

The most obvious manifestation of water-induced plasticization in epoxy networks is a T_g-depression, typically from 10 to 20 °C per wt.% of absorbed water in epoxies [1,2]. The intuitive explanation of this decrease in T_g involves the disruption of intermolecular H-bonds resulting in an increase in molecular mobility [3]. From the molecular mobility standpoint, dynamic mechanical analysis (DMA) and broadband dielectric spectroscopy (BDS) were used to analyze the influence of water sorption on the various relaxations of epoxies. Studies focusing on the sub-T_g molecular mobilities showed that the strength of the β and γ relaxations were strongly dependent on the water content in the epoxy network, which indicated that water molecules H-bonded to the hydroxyl (β-mode) and amine and ether (γ-mode) groups of the epoxy chain [4–6]. Water sorption was also reported to magnify an intermediate mode of delocalized mobility, called ω, often associated with regions of low crosslinking density (or heterogeneity) through which the water molecules preferentially diffuse [7–9]. Finally, a shift towards lower temperatures of the α-relaxation (associated with the glass transition) was evidenced, consistently with the T_g-depression [10,11]. A decrease in the loss peak area at the α-relaxation has been found to accompany the shift towards lower temperatures [12,13] (DMA studies), with various interpretations involving either the water molecules occupying the free volume [14] or the disruption of intermolecular H-bonds [12].

When it comes to studying the influence of absorbed water on the properties of a polymer sample, the main issue is the unstable hydration level over the course of the experiment. In particular, the usual experimental techniques for analysing the molecular mobility thermally probe the sample, which worsens the desorption problem and can cause misleading effects. For instance, the splitting of the α-relaxation of epoxy samples (DMA experiments) into a bimodal loss peak have been reported as a consequence of water-induced plasticization [10,15], but it was shown to mainly be the consequence of water desorption, the sample progressively returning to dry conditions during the experiment [16]. In the literature, polymer samples are usually considered "dry" when they have in fact been stored in the lab environment (allowing ambient moisture to be absorbed), and high hydration states are difficult to maintain during characterization due to the desorption process.

In the present work, we performed *in situ* dielectric measurements, in

* Corresponding author. Université de Lyon, CNRS, UMR 5223, Ingénierie des Matériaux Polymères, UCBL, INSA, UJM, F-69621, Villeurbanne Cedex, France.
E-mail address: aurelien.roggero@insa-lyon.fr (A. Roggero).

https://doi.org/10.1016/j.polymer.2022.124542

continuous immersion, by means of an electrochemical impedance spectroscopy setup optimized for dielectric rather than electrochemical measurements. This setup, presented elsewhere [17], was previously used to study the temperature-activated water sorption kinetics in an epoxy coating [18] and allowed observing its α-relaxation. Differential scanning calorimetry (DSC), BDS and thermally stimulated currents (TSC) were also used to complement the experiments in continuous immersion. For these three techniques, various hydration states of the samples were studied, namely dry (water actively removed from the sample), ambient equilibrated (stored in the lab environment) and wet (removed from immersion). In correlating the influence of these various hydration states, this article aims at further analysing the influence of absorbed water on the molecular mobility modes of an epoxy system, without being restricted by water desorption during the experiment.

2. Experimental

2.1. Polyepoxy samples

A two-component high-solids polyepoxy varnish was manufactured by Peintures Maestria (Pamiers, France). It consisted of an epoxide as base and a mixture of polyamidoamines as hardener. The varnish was deposited by air spraying onto S235JR steel plates (200 mm × 100 mm × 3 mm). Prior to spraying, the steel plates were sand-blasted to an average roughness of 8 ± 1 μm. After 21 days of cure at room temperature (21 °C in a climate-controlled room), the sample thicknesses were in the range of 180 ± 15 μm, as measured by an ultrasonic probe. Freestanding films (for DSC experiments only) were also bar coated onto polypropylene substrates and peeled after cure, with a final thickness of 200 ± 20 μm. In order to stabilize the physicochemical structure (elimination of residual solvent and completion of the crosslinking process), a post-curing step was performed in an oven at 160 °C for 30 min for both the supported and the freestanding films. The post-cured epoxy network was studied in four different states, from dry to continuous immersion in a 0.5 M NaCl aqueous solution, for consistency with the electrochemical impedance spectroscopy measurements that require an electrolytic solution. The associated sample nomenclature is reported in Table 1. In a previous work [18], we estimated the water fraction at saturation to range from 1.2 to 2.5 vol% depending on the temperature (between 20 and 80 °C).

2.2. Differential scanning calorimetry (DSC)

Differential scanning calorimetry measurements were carried out with a Q2000 calorimeter (by TA Instruments) using Tzero™ pans, and after full calibration with sapphire references. Small pieces of an *ambient-equilibrated* freestanding film were cut out to a total mass of approximately 10 mg and put in an aluminium pan, the lid of which was not hermetically sealed, to allow water desorption. A 10 mg-sample was also harvested from a piece of film that had been immersed at 70 °C for 2 h, in order to reach water saturation. This *wet* sample was sealed in a hermetic pan with a 10 μL droplet for the vapour pressure of water inside the pan to prevent desorption from the sample. Three temperature ramps were applied to each sample (heating, cooling, heating) at 20 K/min under a helium flow. The temperature range for the analysis of the dry sample was [50; 150] °C. For the wet sample, it was limited to [5; 80] °C to prevent water from freezing (below 0 °C) and vaporizing (100 °C), the latter representing a significant risk of damaging the DSC apparatus. The glass transition temperatures were determined at the maximum of the derivative heat flow peak.

Table 1
Nomenclature of the different states of the epoxy sample. All the samples are post-cured (160 °C, 30 min).

Dry	The analysis is performed just after the sample was post-cured to prevent moisture ingress.	DSC, BDS
Ambient equilibrated	The sample is equilibrated in the lab environment (~50% RH and 20 °C) prior to the analysis.	DSC, BDS, TSC
Wet	The sample is immersed until water saturation is reached and removed from immersion prior to analysis.	DSC, BDS, TSC
Immersed	The sample is immersed until water saturation is reached and the analysis is performed while the sample is in continuous immersion.	EIS

2.3. Broadband dielectric spectroscopy (BDS)

Electrical impedance measurements were performed with a BDS apparatus (Alpha-A high performance frequency analyser by Novocontrol), in the temperature range [150; 180] °C and in the frequency range [5×10^{-2}; 10^{6}] Hz (with 1.5 V peak voltage amplitude, 9 points acquired per decade). A cylindrical brass electrode (40 mm diameter) was placed on top of a *dry* or *ambient equilibrated* epoxy sample, in the supported film configuration, the steel substrate acting as the lower electrode for the dielectric measurements. The complex dielectric permittivity, $\varepsilon^*(\omega)$, was determined by the WinDeta software, based on Eqs. (1) and (2).

$$\varepsilon^*(\omega) \quad \varepsilon'(\omega) \quad i\,\varepsilon''(\omega) \quad \frac{1}{i\,C_v\,Z^*(\omega)} \tag{1}$$

$$\text{with } C_v \quad \frac{\varepsilon_v \mathscr{A}}{\ell} \tag{2}$$

where $\omega \quad 2\pi f$ is the angular frequency of the applied voltage, $Z^*(\omega)$ the measured complex impedance of the sample, and C_v the capacitance of the equivalent vacuum-filled (ε_v is the vacuum permittivity) parallel plate capacitor formed by two electrodes of area $\mathscr{A}$ (here, the area of the 40 mm top electrode) separated by the distance ℓ (here, the coating thickness).

The Havriliak-Negami parametric equation (Eq. (3)) was used to fit the BDS results in the complex domain and determine the relaxation times [19].

$$\varepsilon^*_{HN}(\omega) \quad \varepsilon_\infty + \frac{\Delta\varepsilon}{(1+(i\ \omega\ \tau_{HN})^\alpha)^\beta} \tag{3}$$

where ε_∞ is the high-frequency limit of the real dielectric permittivity, $\Delta\varepsilon$ the relaxation strength, τ_{HN} the mean relaxation time, α and β shape parameters respectively controlling the width and asymmetry of the distribution.

2.4. Thermally stimulated currents (TSC)

TSC measurements were performed on *wet* and *ambient equilibrated* epoxy samples, which were cut from a coated steel plate into 1 cm^2 diameter cylinders. A matching 1 cm^2 stainless steel cylindrical was used as the complementary top electrode. The sample were placed inside a liquid nitrogen flow cryostat. The sample temperature was controlled by means of an internal heating element, an Eurotherm controlling the power supplied to the heating element, and a Pt100 sensor located in the close vicinity of the sample. The sample chamber was filled with helium gas to enhance thermal exchanges with the sample. Elementary depolarization currents were measured following the fractional polarization procedure detailed in Ref. [20], with 5 °C temperature windows. For each polarization temperature, T_p, in the range [20; 25] °C for *wet* samples and [35; 75] °C for *dry* samples, an electric field was applied to the sample during 2 min. This field was in the linear range: 1.3 MV/m for the *ambient equilibrated* sample and 2.7 MV/m for the *wet* sample (due to weaker depolarization currents). After the polarization step, the temperature was decreased by 5 °C at which point the sample was placed in

short circuit for 2 min. The temperature was then further decreased by 20 °C whilst maintaining the sample in short circuit. Finally, a heating ramp of 7 °C/min was applied up to above T_p (limited to 40 °C for *wet* samples, to limit desorption) whilst acquiring the depolarization currents.

2.5. Electrochemical impedance spectroscopy (EIS)

Impedance measurements were performed in continuous immersion (*immersed* samples), with a REF600+ impedance analyser (by Gamry Instruments). Similarly to the BDS measurements, the steel substrate acted as the working electrode and a graphite rod partially immersed in the electrolyte acted as both the counter and reference electrodes (two electrodes configuration). The main interest of using this technique on polymer samples is the fact that the upper electrode is an aqueous solution, therefore ensuring complete immersion during the impedance measurements. The sample temperature was finely controlled (± 0.5°C stability) by using a Corio CD-200F refrigerated/heating circulator (by Julabo) circulating through a double-jacketed glass cell sealed on top of the sample with a rubber gasket and a clamping system. A Pt100 probe was used to accurately monitor the solution temperature close to the sample without interfering in the electrical measurements. Isothermal impedance measurements were performed in the temperature range [22; 75] °C, from high to low temperatures. The measurement frequency range was [10^{-3}; 10^{6}] Hz for the low temperature isotherms and [3×10^{-3};10^{6}] Hz for those above 50 °C, with a 500 mV_{rms} applied voltage and 10 points acquired per decade. Noteworthily, no evidence of corrosion was observed at any time during the experiments, neither visually nor in the impedance spectra. The complex dielectric permittivity of the immersed epoxy sample was derived from the complex impedance data thanks to Eq. (1), in which $\mathscr{A}$ was the area exposed to the electrolytic solution (34.2 cm^2).

3. Results and discussion

3.1. Water-induced plasticization

DSC was used in the glass transition region of the epoxy network, in both the initially *wet* and *ambient equilibrated* states. For each sample, two heating and one cooling scans were performed and plotted in Fig. 1.

First of all, the narrower temperature window of the DSC scans for the *wet* sample might mislead into thinking that the glass transition is more spread out than in the *ambient equilibrated* one. However, the full width of the derivative heat flow peak at the glass transition (2nd heating scan) is 25 °C for the *wet* sample and 26 °C for the *ambient equilibrated* one: the two glass transitions are comparably broad. During the first heating scan, both samples experience enthalpy recovery as a result of physical ageing (T_g overshoot) prior to the measurements. In the *ambient equilibrated* one, the enthalpy recovery is followed by a water desorption endotherm (peak maximum in the vicinity of 90 °C), which is irreversible and not present in the 2nd heating scan: the sample is therefore supposed to be *dry*. This endotherm is not observed with the *wet* sample which indicates that the hermetic seal and water droplet allowed the vapour pressure of water to be reached in the pan, hence preventing desorption from the sample. The glass transition temperatures of both samples were determined on the 2nd heating scan, at the maximum of the derivative heat flow peak (not shown) and reported on Fig. 1. The absorbed water results in a 18.5 °C T_g-depression, which can be considered as the full extent of water-induced plasticization. Noteworthily, the heat capacity jump at T_g is 26% smaller in the *wet* sample than in the *dry* one. Fig. 2 features the heat capacity, C_p, of the *dry* and *wet* samples during the second DSC heating scan.

From Fig. 2, the lower ΔC_p of the *wet* sample is mainly due to a lower heat capacity value in the rubbery state, while the glassy heat capacity is much less affected. This is a first indication that absorbed water molecules may have a different influence on the molecular mobility of the epoxy network above and below T_g. This point will be further discussed in light of upcoming additional results (section 3.5).

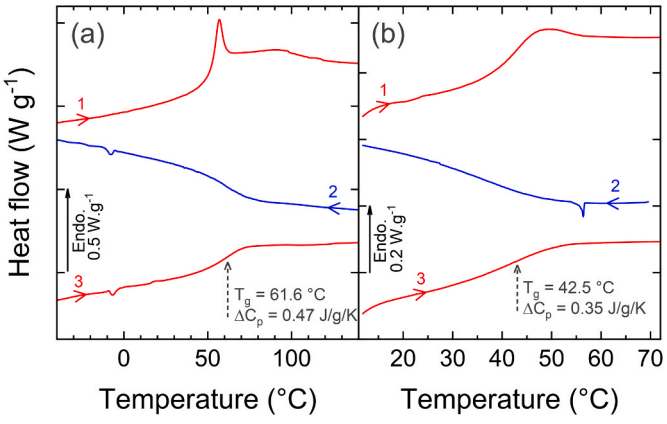

Fig. 1. Differential scanning calorimetry thermograms: *ambient equilibrated* sample (a) and *wet* sample with a water droplet in a hermetic pan (b).

3.2. Molecular mobility modes in the dry state

Broadband dielectric spectroscopy (BDS) measurements were performed on the *dry* epoxy network. The sample was quickly transferred from the post-curing oven to the BDS apparatus which operates under dry nitrogen flow, thus largely limiting the ambient moisture uptake by the sample. A 3D map of the imaginary component of the dielectric permittivity, ε'', is represented in Fig. 3 (as a function of temperature and frequency). Three main molecular mobility modes (α, ω, γ) are annotated in Fig. 3, as well as a high-temperature/low-frequency charge transport contribution (σ).

In the *dry* state (Fig. 3), the γ-mode is distributed over a large temperature range and generally ascribed to the mobility of short aliphatic sequences involving an ether linkage [5]. Noteworthily, no β-mode can be observed in Fig. 3, even though it is usually observed in epoxy samples and generally ascribed to the localized mobility of hydroxyether units and/or phenyl ring flips [21,22]. In this case, the absence of β-mode is explained by the dryness of the sample. We observed on several occasions that after the sample had stayed in ambient conditions for 24 h, the β-mode would clearly be observed by BDS, in the vicinity of 90 °C at 0.1 Hz (see Fig. 1 of [23] for instance). It would however

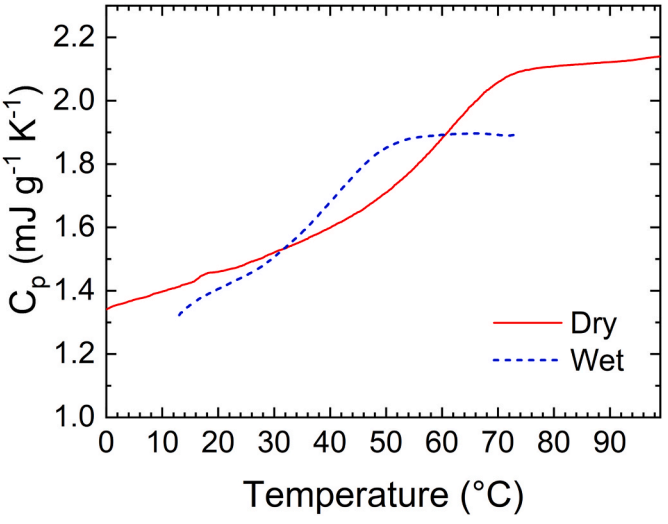

Fig. 2. Heat capacity as a function of temperature for the *dry* and *wet* samples (2nd DSC heating scans).

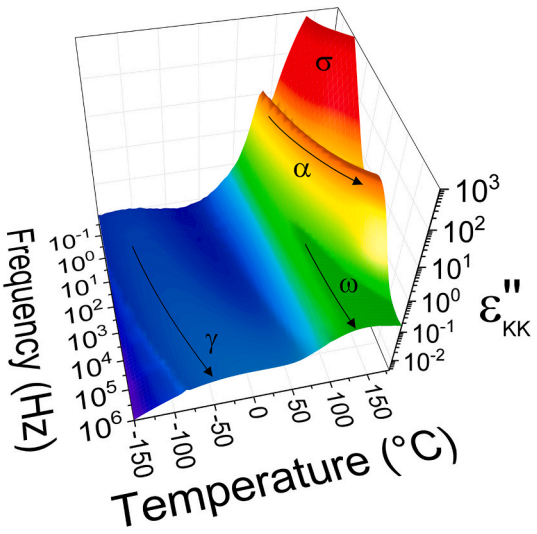

Fig. 3. Dielectric relaxation map in the *dry* state, after applying the Kramers-Kronig relations to the BDS measurements.

disappear again if an additional BDS pass was performed without ambient re-equilibration, hence indicating a strong correlation between the appearance of a β-mode and the presence of absorbed water molecules in this epoxy network. BDS measurements are rarely performed on properly *dry* samples, but rather on *ambient equilibrated* ones that are considered dry. Moreover, it is rare that two successive ramps are performed without ambient re-equilibration because of the need to refill the liquid nitrogen tank. Therefore, some ambient moisture is generally absorbed by epoxy samples, resulting in the appearance of a β-mode.

The α-mode corresponds to the dielectric manifestation of the glass transition, and it was initially strongly convoluted with the charge transport contribution. The application of the Kramers-Kronig relations [24,25] to the real part of the dielectric permittivity yielded a "conduction-free" imaginary part, ε''_{KK} (that is not entirely true because ionic conductivity and electrode polarization also contribute to ε', thus explaining the σ event in Fig. 3). Masked behind the main α-relaxation, another mode is visible at high frequencies. It is probably the so-called ω-mode (it is not associated with a vitreous relaxation and the γ and β relaxations were priorly introduced in the literature), most likely involving the mobility of a more heterogeneous fraction of the epoxy network due to locally lower crosslinking densities [7,26].

3.3. Molecular mobility modes in continuous immersion

Compared to BDS, the accessible temperature window of EIS is narrower (approx. 10 °C–80 °C) because the aqueous solution surrounding the epoxy sample is susceptible to both freezing and vaporization outside this range. The isothermal spectra of the real and imaginary parts of the dielectric permittivity, obtained by EIS measurements in immersion, are plotted in Fig. 4.

While the imaginary component of the permittivity is largely dominated by charge transport processes which mask underlying molecular mobility modes (Fig. 4b), clearly temperature-activated permittivity steps are visible in Fig. 4a. They were ascribed to the α-mode of the epoxy network in a previous study [17]. Less prominent steps are also discernible in the high frequency/low temperature range of the real permittivity (Fig. 4a), and as a peak in the imaginary part (Fig. 4b), both of which shift to higher frequencies when the temperature increases: they are ascribed to the β relaxation (discussion in next section, 3.4). The α-relaxation times were determined by fitting the real permittivity

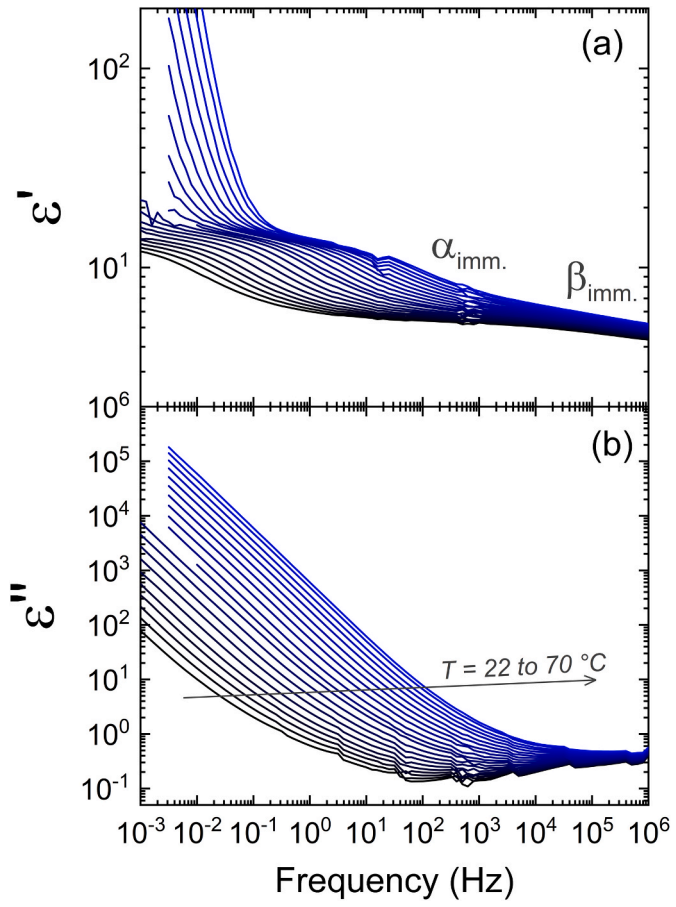

Fig. 4. Real (a) and imaginary (b) parts of the dielectric permittivity measured by EIS on the *immersed* epoxy sample.

spectra with a Havriliak-Negami function, as the dielectric losses due to conduction were too pronounced to involve the imaginary component in the fitting process. For the first two low-temperature isotherms, two Havriliak-Negami terms were used to determine the relaxation times of the β-relaxation as well (Fig. 5). Although the fits were satisfactory, these are just an estimate, as the relaxation is not entirely visible and

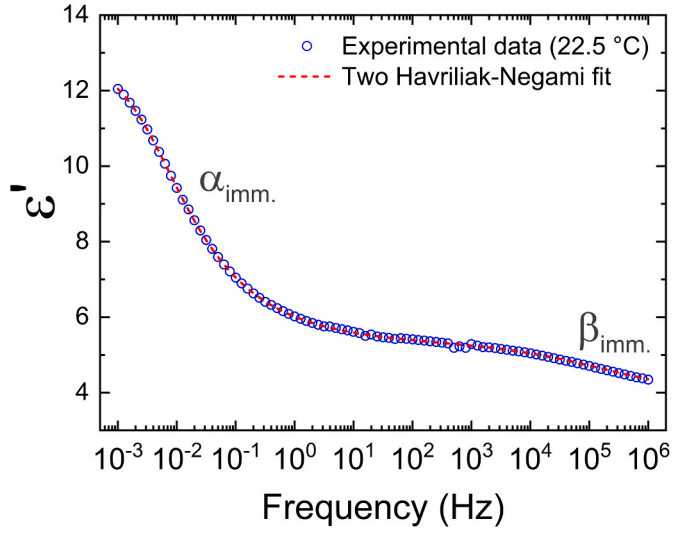

Fig. 5. Real permittivity 22.5 °C-isotherm of the *immersed* sample. Two Havriliak-Negami functions were used to fit both the α and β modes (dashed line).

could extend over a large frequency range (hence only fitting the two lowest temperature isotherms).

3.4. Water influence on the β-relaxation

The β-relaxation times obtained by BDS in the *dry* state and by EIS in continuous immersion are plotted in Fig. 6. The dry β-relaxation times correspond to an *ambient equilibrated* sample (because this mode is not observed with a *dry* sample). The first striking point in Fig. 6 is the good agreement between the two techniques with respect to the β-mode. In first approximation, the relaxation times in the immersed state fall within the Arrhenius extrapolation of the *ambient equilibrated* state, hence justifying the previous attribution of the high-frequency EIS event to the β-relaxation.

The activation energy of the β-mode was obtained by fitting the Arrhenius equation (Eq. (4)) to the *ambient equilibrated* relaxation times.

$$\tau = \tau_0 \, e^{\frac{E_a}{k_B T}} \tag{4}$$

where τ_0 is the pre-exponential factor, E_a the activation energy, k_B the Boltzmann constant and T the temperature.

An activation energy of 64 kJ/mol (0.67 eV) and an average relaxation strength, Δε, of 0.3 were obtained. These values are consistent with the work of Mijović and Zhang on DGEBA-DETA networks [4] (58 kJ/mol and Δε of approx. 0.5), who also reported that while the activation energy was relatively unaffected by water uptake, the relaxation strength increased with water content (0.1 per wt.% of absorbed water). In the immersed case, the average relaxation strength of the β-mode is around 2, which corresponds to a 7-times increase compared to the dry case. Given the imperfect fitting, the order of magnitude seems consistent with the idea that water molecules H-bonded to hydroxyls from the epoxy network are the relaxing entity involved in the β-relaxation of this epoxy network.

3.5. Water influence on the delocalized molecular mobilities

Before analysing the relaxation times, the comparison of relaxation strength, Δε, of the α-relaxation in the *dry* and *immersed* states gives a first indication on how water influences the molecular mobility of the epoxy network. The permittivity steps associated with the α-mode in both states are reported in Fig. 7. The relaxation strength is in the vicinity of 35 for the *dry* sample, which seems high but not inconceivable compared to the literature (20 for a commercial epoxy with 97 °C T_g [27]), and considering both the low T_g and unusual dry conditions. In immersion, the relaxation strength lies in the vicinity of 9, which corresponds to a factor 3.9 between the two states. Absorbed water has a weakening effect on the relaxation strength, more pronounced on the rubbery plateau (low frequency) than in the glassy state, which seems consistent with the (less pronounced) decrease in heat capacity measured by DSC in the rubbery plateau (Fig. 2).

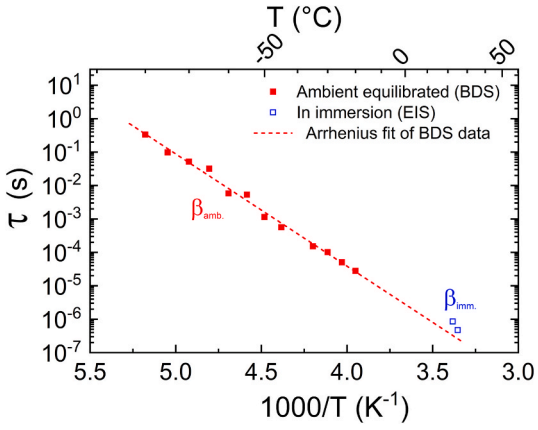

Fig. 6. Arrhenius diagram of the β-relaxation times in the *ambient equilibrated* state (BDS, red filled symbols) and in continuous immersion (EIS, blue open symbols). The Arrhenius fit (*ambient equilibrated*) appears as a red dashed line. (For interpretation of the references to colour in this figure legend, the reader is referred to the Web version of this article.)

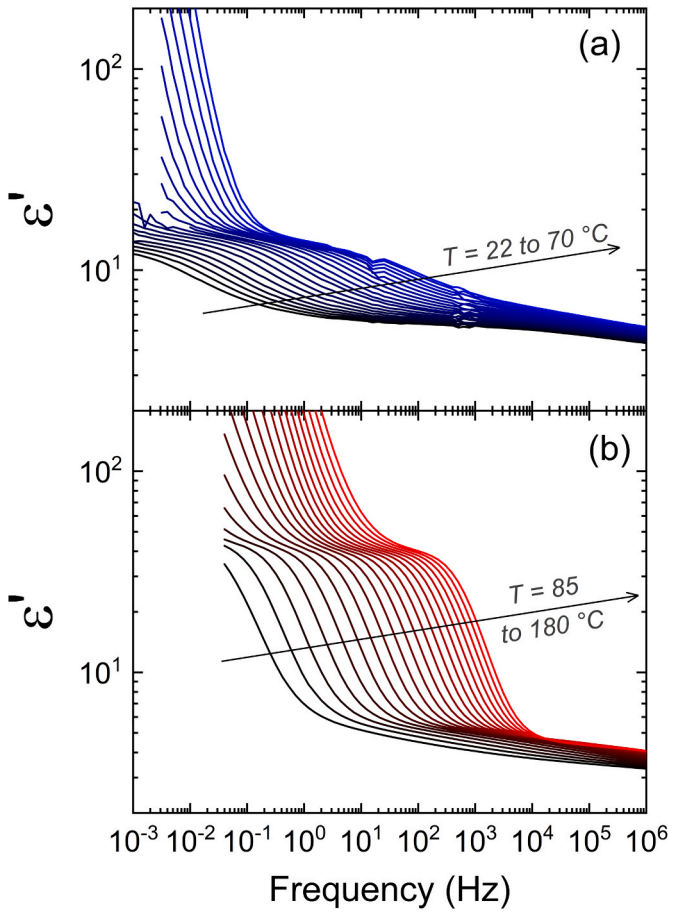

Fig. 7. Real dielectric permittivity steps associated with the α-mode of the epoxy network: *immersed* (EIS) (a) and *dry* (BDS) (b) states.

Elementary thermally stimulated currents thermograms were obtained for a *dry* and a *wet* sample. The depolarization currents were normalized to the sample geometry and polarization voltages, and plotted in Fig. 8. As the immersion was not continuous throughout the experiment, the hydration state was not equivalent to that of EIS measurements. However, thanks to carefully selected temperature ramps (quick equilibrations below 0 °C), the water outtake was limited.

There is a 3.8 ratio between the areas of the two most intense peaks from the *dry* and *wet* samples (Fig. 8), on par with the ratio of the permittivity relaxation strengths from Fig. 7. There are concurring evidences that the absorbed water molecules increase either the number of intermolecular physical bonds involved in the glass transition and/or the motion amplitude of the dipoles in response to the applied electric field. Disruption of intermolecular physical bonds and replacement with H-bond with water molecules is the conventional interpretation of the plasticizing effect [3,28]. The reduction in intermolecular interactions results in the 18.5 °C T_g-depression observed by DSC (Fig. 1) and a shift of the α-mode towards lower temperatures, but is also consistent with the lower relaxation strength.

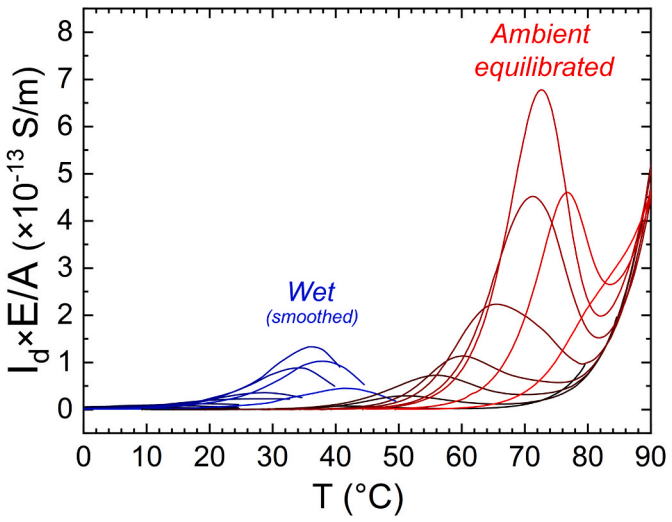

Fig. 8. Elementary TSC peaks, normalized to the electrode area and applied polarizing field, obtained with the fractional polarization method on the *wet* (blue lines) and *ambient equilibrated* samples (red lines). (For interpretation of the references to colour in this figure legend, the reader is referred to the Web version of this article.)

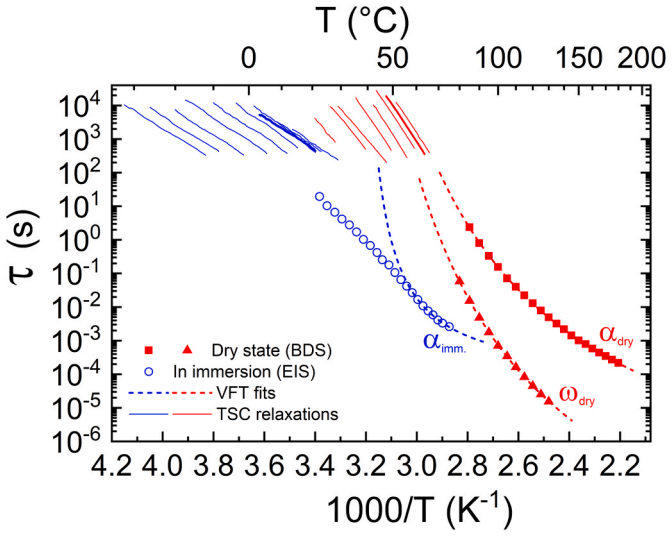

Fig. 9. Arrhenius diagram of the delocalized molecular mobility modes in the *dry* (BDS, filled symbols) and *immersed* (EIS, empty symbols) states. The TSC elementary thermograms of the *ambient equilibrated* and *wet* samples are also reported as lines in the [10^2; 10^4] s range.

We now focus, in Fig. 9, on the relaxation times of the α and ω modes, obtained from TSC (continuous lines in the upper part of the diagram), BDS (filled symbols, from complex Havriliak-Negami fits of ε^*_{KK}) and EIS in immersion (empty symbols).

TSC being an equivalent low-frequency technique (or high τ), the sample is probed in its dynamic glassy state (below the dynamic T_g), hence the relaxation times display Arrhenius dependences with respect to temperature [29–31]. The BDS relaxation times of both the α and ω modes in the *dry* state obey the Vogel-Fulcher-Tammann (VFT) law. The VFT fits are represented in red dashed lines in Fig. 9 and the corresponding fit parameters are reported in Table 2. The most striking element is the behaviour of the α-relaxation times in continuous immersion (EIS measurements, blue empty circles in Fig. 9). On the one hand they display a VFT dependence above 50–60 °C, but on the other hand a straight line, indicative of an Arrhenius dependence, is observed at lower temperatures.

Table 2
Vogel-Fulcher-Tammann fit parameters in the dry state and in immersion.

	τ_0 (s)	α_f (K^{-1})	T_∞ (°C)
Dry α-mode	1.1×10^{7}	7.7×10^{4}	7.9
Dry ω-mode	1.2×10^{10}	7.0×10^{4}	8.3
Immersed α-mode	8.6×10^{5}	7.3×10^{3}	34.8

The Stickel function [32], based on the derivative of $\ln(\tau^{-1})$ with respect to 1/T, was used to confirm the previous statements regarding the temperature dependences of τ (BDS and EIS), and plotted in Fig. 10.

After applying the Stickel function, an Arrhenius dependence becomes a constant value, K, equal to:

$$K \quad \sqrt{\frac{k_B}{E_a}} \tag{5}$$

where k_B is the Boltzmann constant and E_a the Arrhenius activation energy.

A VFT dependence is linearized by the Stickel function, by design. The slope and y-intercept are linked to the VFT parameters according to Eqs. (6) and (7):

$$\text{Slope} \quad T_\infty \sqrt{\alpha_f} \tag{6}$$

$$\text{y-intercept} \quad \sqrt{\alpha_f} \tag{7}$$

where α_f is the thermal expansion coefficient of free volume and T_∞ the Vogel temperature, referring to the free volume approach of the glass transition.

The *dry* α and ω relaxation times clearly show a linear dependence in the Stickel plot (Fig. 10), which confirms their VFT behaviour. For each relaxation, only one VFT law is needed to fit the entire range of τ. The comparable slopes are consistent with the similar values of T_∞ and α_f (Table 2). The *immersed* sample also displays a VFT dependence above 60 °C, with a steeper slope and higher y-intercept value. At temperatures below 60 °C, it is unclear whether a constant value is reached (Arrhenius law) or an increasing linear function of 1/T (which would not have a definite physical meaning). It is worth noting that the differentiation step involved in the Stickel function greatly magnifies the "noise" in the relaxation times which hinders the determination of the low temperature α behaviour for the *immersed* sample. Unfortunately, data

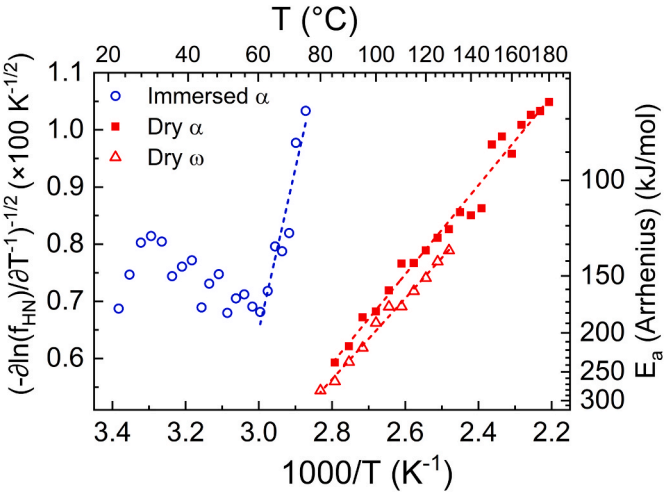

Fig. 10. Stickel plot featuring the α and ω relaxations in the *dry* state (red symbols) and the *wet* α-mode (blue symbols). The linear regressions associated with Vogel-Fulcher-Tammann regimes appear as dashed lines. The right y-axis shows the activation energy associated with a constant value (Arrhenius regime) on the Stickel plot. (For interpretation of the references to colour in this figure legend, the reader is referred to the Web version of this article.)

smoothing prior to or after the differentiation step should be avoided, as it has a significant impact on the outcome.

3.6. VFT to Arrhenius crossover at the dynamic T_g in immersion

We now focus on the apparent Arrhenius dependence of the α-relaxation times in continuous immersion, as measured *in situ* by EIS below 60 °C. From the comparison of the DSC scan and the dielectric relaxation times (Fig. 11), the VFT-Arrhenius crossover seems to be triggered by the glass transition. A linear fit in the Arrhenius diagram (first 10 points of Fig. 11b) yields a mean activation energy of 141 kJ/mol (1.46 eV). The calorimetric T_g (2nd heating ramp) of the *wet* sample is also reported in Fig. 11b, at the equivalent frequency estimated for a 20 K/min ramp [33].

The activation energies were also determined from the elementary TSC peaks in Fig. 8 and reported in Fig. 12 as a function of the temperature at peak maximum. The zero activation entropy line at 1 mHz, as defined by Starkweather [34], was also reported as a dashed line. Localized mobilities (typically in the glassy state) lie close to this line, while an increasing distance from the line indicates increasing cooperativity of the molecular mobility.

The striking feature in Fig. 12 is the close proximity of the TSC activation energies of the *wet* sample (blue circles) to the Starkweather line. This is unexpected because the α-relaxation of polymers is generally cooperative to some extent, as is observed with the *ambient equilibrated* sample (red squares). This suggests that water localises the α mobility and makes it appear like a glassy mode. As indicated by the violet dotted line in Fig. 12, there is a discrepancy between the activation energies obtained by TSC on the *wet* sample (approx. 100 kJ/mol) and that obtained in immersion by EIS (average 140 kJ/mol). This means that the TSC lines and the Arrhenius behaviour in EIS do not perfectly line up in Fig. 9, but this discrepancy should be contextualized with respect to the different timescales involved in the two techniques (lower frequencies with TSC).

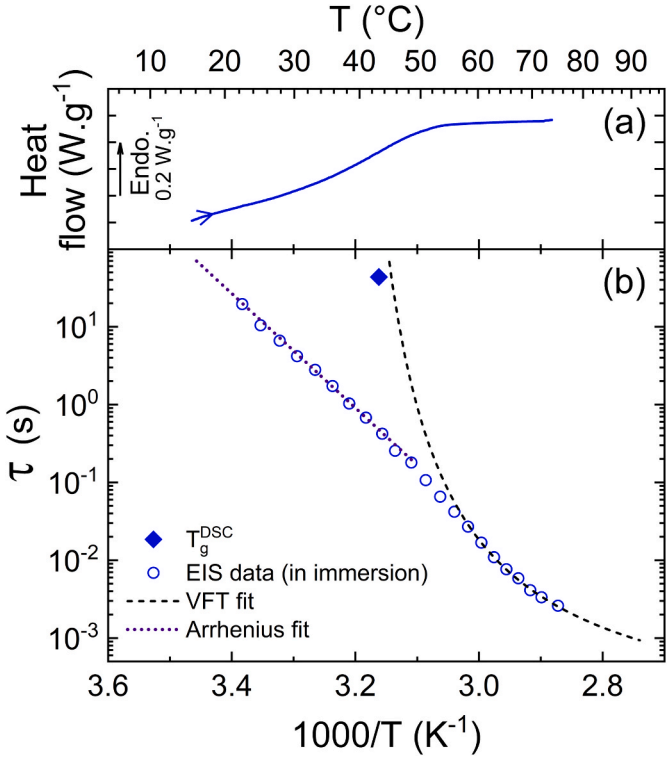

Fig. 11. (a) 2nd heating DSC scan on the *wet* sample and (b) α-relaxation times from EIS measurements on the *immersed* sample and calorimetric T_g (filled diamond).

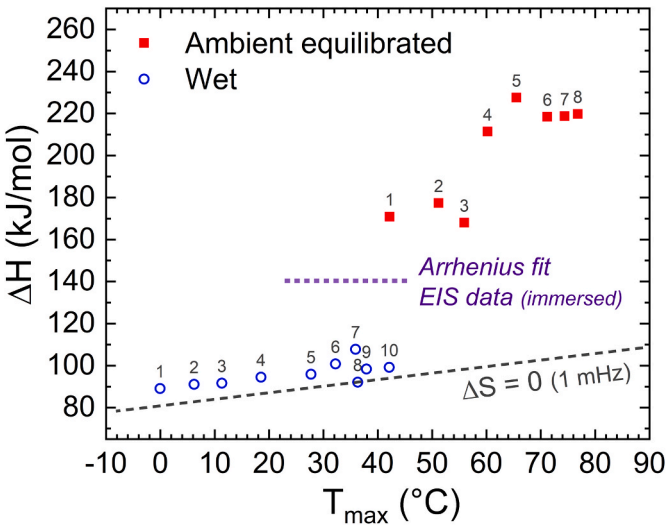

Fig. 12. Enthalpy of relaxation as extracted from thermally stimulated depolarization currents on the *ambient equilibrated* and *wet* samples. The calculated zero entropy line (at 1 mHz) is displayed as a grey dashed line. The mean activation energy of the low-temperature EIS points (*immersed* sample) is reported as a purple dotted line. (For interpretation of the references to colour in this figure legend, the reader is referred to the Web version of this article.)

4. Discussion

Above the wet T_g of the epoxy network, the α mobility corresponds to the expected plasticized behaviour, that is a VFT dependence of τ but shifted towards the lower temperatures (Fig. 9). Consistently with the decrease in the loss peak area at the α-relaxation in DMA, reported in the literature [12,13], the amplitude of the various manifestations of the glass transition – ΔC_p (Fig. 2), Δε' (Fig. 7), TSC peak areas (Fig. 8) – all decreased consequently to the absorption of water. Each of these events is correlated to the amount of conformational degrees of freedom of the main chain gained upon heating (or lost upon cooling) through the glass transition. Qualitatively, the H-bonded water molecules probably form a dynamic physical network which limits the degrees of freedom of the epoxy network. This reduction in degrees of freedom is somewhat counterintuitive because the decrease in T_g is usually seen as an enhancement of molecular mobility (faster dynamics), but in this case, the amount of relaxation is also decreased.

As the temperature is decreased below the wet T_g, there is a drastic change in the temperature dependence of τ to a seemingly Arrhenius dependence (Fig. 9), although not unambiguously confirmed by the Stickel plot (Fig. 10). Several possible explanations of this change in behaviour come to mind; they are developed in the following part of the discussion.

Firstly, perhaps the most intuitive explanation for this crossover would be that the epoxy networks falls out of equilibrium upon cooling below T_g, which results in a slowing down of the α-relaxation times. The existence of this theoretically anticipated crossover is still discussed in the community [35,36], and it is not clearly observed in the vast majority of experimental studies, especially those based on BDS measurements. The relaxation times indeed become too long to be observed in the frequency range of the technique (usually 10^{-2} to 10^6 Hz) [37]. In the present case, the crossover was not observed with the *ambient equilibrated* or *dry* samples, and it is unclear how it could become observable solely as a consequence of immersion (the *dry* network should also fall out of equilibrium at some point). Another inconsistency with this scenario is the fact that the calorimetric T_g of the *immersed* sample is far from lining up with the dielectric relaxation times (Fig. 11b), as should be the case if the crossover was intrinsic to the epoxy network.

Secondly, the VFT to Arrhenius crossover in the vicinity of T_g echoes physical aging studies reporting a double decay in the enthalpy recovery of glasses aged below enough T_g [38,39]. In particular, by analysing the time of equilibration of these two processes in polystyrene, Cangialosi et al. proposed a splitting scenario of the dynamics occurring upon cooling through T_g, the slowest of which was associated with the α-relaxation following a VFT law and the fastest with an alternative molecular mechanism possibly involving secondary relaxations [38]. A similar interpretation could apply to our results on *immersed* samples, where the fast mechanism below T_g might be emphasized by the absorbed water molecules interacting with the network. However, the techniques used in the present work do not allow us to confirm such mechanism is operating in the studied polymer system.

Thirdly, the change in the temperature dependence of the relaxation times observed in the water saturated sample could also result from a "water-induced confinement". Several articles from a group of the *Centro de Física de Materiales* (Spain) reported VFT to Arrhenius crossovers in the molecular mobility of water in a variety of systems, *e.g.* graphite oxide [40], polymer mixtures [41], studied by BDS. The authors ascribed the transition to an Arrhenius dependence at low temperatures to confinement effects on the water molecules, either due to geometrical restrictions, or in a polymer matrix below T_g. In the latter case, the crossover took place at the T_g of the water-polymer mixture. In the present work, the dielectric relaxation showing the crossover phenomenon is observed at too high temperatures (above 0 °C) to be associated with a mobility mode of the water molecules.

While a glassy polymer matrix can confine the mobility of water molecules, perhaps the mobility of the epoxy network saturated with water (in immersion) could inversely be somewhat confined by the interaction with H-bond water molecules. Barroso-Bujans et al. [42] reported a VFT to Arrhenius crossover phenomenon with Poly(Ethylene Oxide) confined in the nanopores of resorcinol-formaldehyde nanoparticles. They ascribed the crossover phenomenon to the freezing of long-living H-bonds at the pore surface below the crossover temperature, which limited the cooperativity of the α mobility. Lorthioir et al. reported a speeding up and localization of the dynamics of PVME in PVME-PS mixtures [43]. Following a similar thinking pattern, they ascribed it to the freezing of the segmental dynamics of PS below T_g in turn constraining the mobility of PVME. A similar scenario could apply to the present case of the water-saturated epoxy, where the H-bonds are formed between the –OH groups of the network and the water molecules that fill the accessible volume.

Water saturation is thought to be a governing factor in the observation of such a crossover, as it seems that it was not reported with polymer samples exposed to various water activities (but no saturation), and molecular mobility is rarely probed in continuous immersion. Intuitively, the need for water to saturate the entire available space in the polymer network for it to induce significant confinement effects makes sense. The present results highlight the value of performing *in situ* dielectric experiments, and the original molecular mobility behaviour in complete immersion could provide new insights in some fundamental aspects of the glass transition.

5. Conclusions

The molecular mobilities of an epoxy network were probed by dielectric measurements in continuous immersion, and compared to the dry state. The usual plasticization effect (T_g-depression, shift of the α-relaxation towards lower temperatures) was accompanied by an unconventional crossover from a Vogel-Tammann-Fulcher behaviour to an Arrhenius dependence as the temperature decreased in the vicinity of the plasticized T_g. A study of the thermally stimulated currents evidenced the localized nature of the mobility associated with the glass transition in the wet sample. All these observations could be the result of the water molecules restricting the mobility of the epoxy network by H-bond and inducing confinement effects.

This work showed that performing temperature activated dielectric measurements in continuous immersion allowed probing the molecular mobility of epoxy samples in high plasticization states, that are not attainable by conventional techniques such as DMA or BDS, where the hydration state cannot be maintained constant throughout the measurement. We hope to consolidate this methodology by applying it to other polymer systems (the T_g of which lies within the temperature range [30; 60] °C), which will also help to confirm the hypotheses formulated about the localization of the α mobility by the H-bonds between the network and the water molecules. *In situ* dielectric measurements, such as described in this work, may provide new leads in the interpretation of the molecular mobility of polymers plasticized by water, and could potentially help clarifying some fundamental aspects of the glass transition.

CRediT authorship contribution statement

Aurélien Roggero: Conceptualization, Data curation, Formal analysis, Investigation, Methodology, Writing – original draft. **Nicolas Caussé:** Conceptualization, Formal analysis, Methodology, Supervision, Validation, Writing – review & editing. **Nadine Pébère:** Conceptualization, Formal analysis, Methodology, Supervision, Validation, Writing – review & editing, Project administration. **Eric Dantras:** Conceptualization, Formal analysis, Methodology, Supervision, Validation, Writing – review & editing, Project administration.

Declaration of competing interest

The authors declare that they have no known competing financial interests or personal relationships that could have appeared to influence the work reported in this paper.

References

[1] T.S. Ellis, F.E. Karasz, Interaction of epoxy resins with water: the depression of glass transition temperature, Polymer 25 (1984) 664–669, https://doi.org/10.1016/0032-3861(84)90034-X.

[2] E. Linde, N.H. Giron, M.C. Celina, Water diffusion with temperature enabling predictions for sorption and transport behavior in thermoset materials, Polymer 153 (2018) 653–667, https://doi.org/10.1016/j.polymer.2018.08.024.

[3] J. Zhou, J.P. Lucas, Hygrothermal effects of epoxy resin. Part I: the nature of water in epoxy, Polymer 40 (1999) 5505–5512, https://doi.org/10.1016/S0032-3861(98)00790-3.

[4] J. Mijović, H. Zhang, Local dynamics and molecular origin of polymer network-water interactions as studied by broadband dielectric relaxation spectroscopy, FTIR, and molecular simulations, Macromolecules 36 (2003) 1279–1288, https://doi.org/10.1021/ma021568q.

[5] J.M. Pochan, R.J. Gruber, D.F. Pochan, Dielectric relaxation phenomena in a series of polyhydroxyether copolymers of bisphenol-A—endcapped polyethylene glycol with epichlorohydrin, J. Polym. Sci. Polym. Phys. Ed 19 (1981) 143–149, https://doi.org/10.1002/pol.1981.180190112.

[6] C. Maggana, P. Pissis, TSDC studies of the effects of plasticizer and water on the sub-T g relaxations of an epoxy resin system, J. Macromol. Sci. Part B. 36 (1997) 749–772, https://doi.org/10.1080/00222349708212400.

[7] J.D. Keenan, J.C. Seferis, J.T. Quinlivan, Effects of moisture and stoichiometry on the dynamic mechanical properties of a high-performance structural epoxy, J. Appl. Polym. Sci. 24 (1979) 2375–2387, https://doi.org/10.1002/app.1979.070241206.

[8] P. Zinck, J.F. Gérard, Polyepoxide-water interactions: influence of the chemical structure of the network, Polym. Degrad. Stabil. 93 (2008) 1231–1237, https://doi.org/10.1016/j.polymdegradstab.2007.11.013.

[9] J.-Y. Wang, H.J. Ploehn, Dynamic mechanical analysis of the effect of water on glass bead-epoxy composites, J. Appl. Polym. Sci. 59 (1996) 345–357, https://doi.org/10.1002/(SICI)1097-4628(19960110)59:2<345::AID-APP19>3.0.CO;2-V.

[10] C. Grave, I. McEwan, R.A. Pethrick, Influence of stoichiometric ratio on water absorption in epoxy resins, J. Appl. Polym. Sci. 69 (1998) 2369–2376.

[11] G. Xian, V.M. Karbhari, DMTA based investigation of hygrothermal ageing of an epoxy system used in rehabilitation, J. Appl. Polym. Sci. 104 (2007) 1084–1094, https://doi.org/10.1002/app.25576.

[12] G. Xian, V.M. Karbhari, Segmental relaxation of water-aged ambient cured epoxy, Polym. Degrad. Stabil. 92 (2007) 1650–1659, https://doi.org/10.1016/j.polymdegradstab.2007.06.015.

[13] A. Le Guen-Geffroy, P.Y. Le Gac, B. Habert, P. Davies, Physical ageing of epoxy in a wet environment: coupling between plasticization and physical ageing, Polym. Degrad. Stabil. 168 (2019) 108947, https://doi.org/10.1016/j.polymdegradstab.2019.108947.

[14] P. Nogueira, C. Ramírez, A. Torres, M.J. Abad, J. Cano, J. López, I. López-Bueno, L. Barral, Effect of water sorption on the structure and mechanical properties of an epoxy resin system, J. Appl. Polym. Sci. 80 (2001) 71–80, https://doi.org/10.1002/1097-4628(20010404)80:1<71::AID-APP1077>3.0.CO;2-H.
[15] O. Starkova, S.T. Buschhorn, E. Mannov, K. Schulte, A. Aniskevich, Water transport in epoxy/MWCNT composites, Eur. Polym. J. 49 (2013) 2138–2148, https://doi.org/10.1016/j.eurpolymj.2013.05.010.
[16] A. Chateauminois, B. Chabert, J.P. Soulier, L. Vincent, Dynamic mechanical analysis of epoxy composites plasticized by water: artifact and reality, Polym. Compos. 16 (1995) 288–296, https://doi.org/10.1002/pc.750160405.
[17] A. Roggero, N. Caussé, E. Dantras, L. Villareal, A. Santos, N. Pébère, Thermal activation of impedance measurements on an epoxy coating for the corrosion protection: 2. Electrochemical impedance spectroscopy study, Electrochim. Acta 305 (2019) 116–124, https://doi.org/10.1016/j.electacta.2019.03.007.
[18] A. Roggero, N. Caussé, E. Dantras, L. Villareal, A. Santos, N. Pébère, In situ study of the temperature activated kinetics of water sorption in an epoxy varnish, Polymer 213 (2021) 123206, https://doi.org/10.1016/j.polymer.2020.123206.
[19] S. Havriliak, S. Negami, A complex plane analysis of α-dispersions in some polymer systems, J. Polym. Sci. Part C Polym. Symp. 14 (1966) 99–117, https://doi.org/10.1002/polc.5070140111.
[20] G. Teyssedre, C. Lacabanne, Some considerations about the analysis of thermostimulated depolarization peaks, J. Phys. D Appl. Phys. 28 (1995) 1478–1487, https://doi.org/10.1088/0022-3727/28/7/029.
[21] N. Causse, E. Dantras, C. Tonon, M. Chevalier, H. Combes, P. Guigue, C. Lacabanne, Enthalpy relaxation phenomena of epoxy adhesive in operational configuration: thermal, mechanical and dielectric analyses, J. Non-Cryst. Solids 387 (2014) 57–61, https://doi.org/10.1016/j.jnoncrysol.2013.12.028.
[22] J.G. Williams, The beta relaxation in epoxy resin-based networks, J. Appl. Polym. Sci. 23 (1979) 3433–3444, https://doi.org/10.1002/app.1979.070231201.
[23] A. Roggero, N. Caussé, E. Dantras, L. Villareal, A. Santos, N. Pébère, Thermal activation of impedance measurements on an epoxy coating for the corrosion protection: 1. Dielectric spectroscopy response in the dry state, Electrochim. Acta 305 (2019) 116–124, https://doi.org/10.1016/j.electacta.2019.02.035.
[24] P.A.M. Steeman, J. Van Turnhout, A numerical Kramers-Kronig transform for the calculation of dielectric relaxation losses free from Ohmic conduction losses, Colloid Polym. Sci. 275 (1997) 106–115.
[25] J. van Turnhout, Better resolved low frequency dispersions by the apt use of kramers-kronig relations, differential operators, and all-in-1 modeling, Front. Chem. 4 (2016) 1–19, https://doi.org/10.3389/fchem.2016.00022.
[26] M. Chevalier, E. Dantras, C. Tonon, P. Guigue, C. Lacabanne, C. Puig, C. Durin, Correlation between sub-T g relaxation processes and mechanical behavior for different hydrothermal ageing conditions in epoxy assemblies, J. Appl. Polym. Sci. 115 (2010) 1208–1214, https://doi.org/10.1002/app.31253.
[27] H. Hammami, M. Arous, M. Lagache, A. Kallel, Study of the interfacial MWS relaxation by dielectric spectroscopy in unidirectional PZT fibres/epoxy resin composites, J. Alloys Compd. 430 (2007) 1–8, https://doi.org/10.1016/j.jallcom.2006.04.048.
[28] M.J. Adamson, Thermal expansion and swelling of cured epoxy resin used in graphite/epoxy composite materials, J. Mater. Sci. 15 (1980) 1736–1745, https://doi.org/10.1007/BF00550593.
[29] J. van Turnhout, Thermally stimulated discharge of electrets, in: G.M. Sessler (Ed.), Electrets, second ed., Springer-Verlag, New York, 1987, pp. 81–215.
[30] C. Lacabanne, A. Lamure, G. Teyssedre, A. Bernes, M. Mourgues, Study of cooperative relaxation modes in complex systems by thermally stimulated current spectroscopy, J. Non-Cryst. Solids 172–174 (1994) 884–890, https://doi.org/10.1016/0022-3093(94)90593-2.
[31] A. Alegría, L. Goitiandía, J. Colmenero, On the interpretation of the TSDC results in the study of the α-relaxation of amorphous polymers, Polymer 37 (1996) 2915–2923, https://doi.org/10.1016/0032-3861(96)89387-6.
[32] F. Stickel, E.W. Fischer, R. Richert, Dynamics of glass-forming liquids. I. Temperature-derivative analysis of dielectric relaxation data, J. Chem. Phys. 102 (1995) 6251, https://doi.org/10.1063/1.469071.
[33] A. Hensel, J. Dobbertin, J.E.K. Schawe, A. Boller, C. Schick, Temperature modulated calorimetry and dielectric spectroscopy in the glass transition region of polymers, J. Therm. Anal. Calorim. 46 (1996) 935–954.
[34] H.W. Starkweather, Simple and complex relaxations, Macromolecules 14 (1981) 1277–1281, https://doi.org/10.1021/ma50006a025.
[35] G.B. McKenna, S.L. Simon, 50th anniversary perspective: challenges in the dynamics and kinetics of glass-forming polymers, Macromolecules 50 (2017) 6333–6361, https://doi.org/10.1021/acs.macromol.7b01014.
[36] V.N. Novikov, A.P. Sokolov, Qualitative change in structural dynamics of some glass-forming systems, Phys. Rev. E. 92 (2015) 1–8, https://doi.org/10.1103/PhysRevE.92.062304.
[37] G.B. McKenna, Glass dynamics: diverging views on glass transition, Nat. Phys. 4 (2008) 673–674, https://doi.org/10.1038/nphys1063.
[38] D. Cangialosi, V.M. Boucher, A. Alegría, J. Colmenero, Direct evidence of two equilibration mechanisms in glassy polymers, Phys. Rev. Lett. 111 (2013) 1–5, https://doi.org/10.1103/PhysRevLett.111.095701.
[39] A. Morvan, N. Delpouve, A. Vella, A. Saiter-Fourcin, Physical aging of selenium glass: assessing the double mechanism of equilibration and the crystallization process, J. Non-Cryst. Solids 570 (2021) 121013, https://doi.org/10.1016/j.jnoncrysol.2021.121013.
[40] S. Cerveny, F. Barroso-Bujans, Á. Alegría, J. Colmenero, Dynamics of water intercalated in graphite oxide, J. Phys. Chem. C 114 (2010) 2604–2612, https://doi.org/10.1021/jp907979v.
[41] S. Cerveny, Á. Alegría, J. Colmenero, Universal features of water dynamics in solutions of hydrophilic polymers, biopolymers, and small glass-forming materials, Phys. Rev. E. 77 (2008) 1–5, https://doi.org/10.1103/PhysRevE.77.031803.
[42] F. Barroso-Bujans, S. Cerveny, P. Palomino, E. Enciso, S. Rudić, F. Fernandez-Alonso, A. Alegria, J. Colmenero, Dynamics and structure of poly(ethylene oxide) intercalated in the nanopores of resorcinol-formaldehyde resin nanoparticles, Macromolecules 49 (2016) 5704–5713, https://doi.org/10.1021/acs.macromol.6b01285.
[43] C. Lorthioir, A. Alegría, J. Colmenero, Out of equilibrium dynamics of poly(vinyl methyl ether) segments in miscible poly(styrene)-poly(vinyl methyl ether) blends, Phys. Rev. E. 68 (2003) 9, https://doi.org/10.1103/PhysRevE.68.031805.